Railton, C. J. (2015). A Tilted Subgrid for Two Dimensional FDTD. In 2015 9th European Conference on Antennas and Propagation (EuCAP 2015): Proceedings of a meeting held 13-17 April 2015, Lisbon, Portugal. (pp. 1-5). (Proceedings of the European Conference on Antennas and Propagation). Institute of Electrical and Electronics Engineers (IEEE).

Peer reviewed version

A Tilted Subgrid for Two Dimensional FDTD

Chris J Railton[1]
[1] Centre for Communications Research, University of Bristol, Bristol, England, chris.railton@bristol.ac.uk

***Abstract*—Although the Finite Difference Time Domain (FDTD) method is well established for addressing a wide variety problems including the characterization of antenna arrays, a long standing challenge is to reduce discretization errors while avoiding the use of impractically large numbers of cells, particularly when the structure is large and contains regions of fine detail. One solution is to use subgrids. In most published work, Cartesian subgrids are proposed which are in the same orientation as the main grid. However there is considerable benefit to allowing for the subgrid to be tilted. In this work, a method for introducing a tilted subgrid into the 2D FDTD mesh is presented and its effectiveness, accuracy and stability is demonstrated using examples. The method is readily extendable to a full 3D implementation.**

***Index Terms*—FDTD methods, subgridding.**

I. INTRODUCTION

The Finite Difference Time Domain (FDTD) method has been widely used to characterize antennas and antenna arrays for several decades. Nevertheless structures which contain fine geometrical detail but which are also electrically large still present a challenge. The difficulty is much greater when the elements of an antenna array are each orientated in a different direction, such is the case in the system described in [1]. In [2] and [3], a method is presented whereby each element of the array is modeled using a Cartesian mesh which is orientated in the most appropriate way for that element. These separate meshes are then rotated and positioned to match the actual location and orientation of each element in the array. This led to a three stage process which allowed the antenna array to be characterized with computational requirements which were several orders of magnitude smaller than would be needed if using direct FDTD methods.

Although good results were obtained, this method makes the approximation that energy is transferred only in one direction, ie. from the excited element to all the non-excited ones and multiple reflections were ignored. When the coupling between elements is small, as in the case of [1], this is appropriate. If the coupling is high, however, then a more rigorous approach is needed.

Recently, a full subgridding method has been presented which is based upon Huygens and anti-Huygens surfaces [4]. Although the method is effective and flexible, it has been applied only to the situation where all the grids are orientated in the same direction such as the case shown in Figure 1. In this contribution, the methods of [3] and [4] are generalized and extended to allow application to subgrids which are tilted, as shown in Figure 2 as well as accounting for the flow of energy in both directions.

II. THEORY

In the proposed method a subgrid, which may be tilted, is placed within the 2 dimensional main grid as shown in Figure 1 or Figure 2. The subgrid, is surrounded by two closed surfaces which are defined as shown in Figure 3. Energy is transferred between the two grids by applying the equivalence principle. Fields impinging on the inner surface from the main grid are replaced by equivalent electric and magnetic currents which are used as excitation sources for the subgrid. This is done using equations (1) and (2).

$$J = \hat{n} \times H \tag{1}$$

$$M = -\hat{n} \times E \tag{2}$$

Similarly the fields impinging on the outer surface from the subgrid are replaced by equivalent electric and magnetic currents which are used as excitation sources for the main grid.

A more detailed illustration is shown in Figure 4 where the lower left part of the boundary between the subgrid and the main grid is shown. The TM case is considered here although the TE case can be similarly treated. The main grid is aligned on the (x,y) axes while the subgrid is aligned with the rotated axis (u,v). The upper pair of lines form the inner surface and the lower pair form the outer surface. For clarity, the only subgrid nodes which are shown are those on the boundary. The E field nodes are shown by crosses and the H field nodes by circles. This arrangement is similar to the one used in [4] except that here there is no restriction on the angle between the grids and none of the subgrid nodes are located at the same point as the main grid nodes. In the first instance, the distance between the inner and outer surfaces was set to 3 times the size of the main grid cell size following [4]. Since the locations of the subgrid nodes are not the same as in the main grid, interpolation and distribution in space is necessary.

A. The Inner surface - interpolation

The inner surfaces consist of two rectangles, parts of which are shown in the upper right hand corner of Figure 4. These surfaces are used to transfer energy from the main grid to the subgrid. This is done as follows:

1. For the position of each E_u or E_v node on the rectangle, shown as red crosses, the value of the H

field in the main grid is found from the surrounding H_z nodes using linear interpolation.
2. Using equation (1), the value of the equivalent electric currents, J_u or J_v, are found for each node.
3. These contributions of these currents are added to the update equations for E_u or E_v respectively.
4. For the position of each H_z node on the rectangle, ahown as blue circles, the value of the E field in the main grid is found from the surrounding E_x and E_y nodes using linear interpolation.
5. Using equation (2), the value of the equivalent magnetic current, M_z is found at each node.
6. These contributions of these currents are added to the update equations for H_z.

B. The Outer surface - distribution

The outer surface consists of the two rectangles in the lower left hand corner of Figure 4. These surfaces are used to transfer energy from the subgrid to the main grid and this is done as follows:

1. For each E_u or E_v node on the rectangle, the value of the equivalent current, M_z, is found using equation (2).
2. This current is shared out to the surrounding H_z nodes in the main grid using the same weightings as were used for the inner surface interpolation.
3. These contributions of these currents are added to the update equations for the H_z nodes.
4. For each H_z node on the rectangle, the value of the equivalent currents, J_u or J_v are found using equation (1).
5. This current is shared out to the surrounding E_x and E_y nodes in the main grid using the same weightings as were used for the inner surface interpolation.
6. The contributions of these currents are added to the update equations for E_x and E_y.

As in [4], time interpolation is also necessary at each iteration and, in order to do this correctly, the nodes near the boundary need to be advanced in time before those in the rest of the mesh. These precursors are calculated in a way analogous to [4] but because the two grids are not aligned, a larger number of nodes need to be advanced. The affected nodes for the example given in Figure 4 are shown in green.

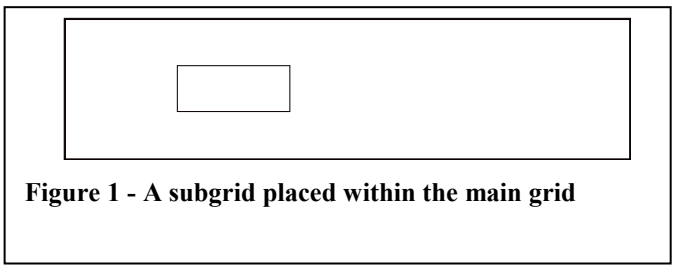

Figure 1 - A subgrid placed within the main grid

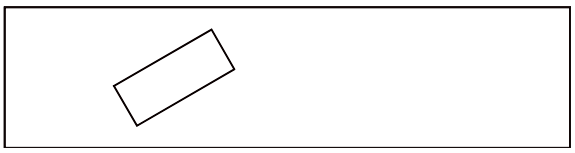

Figure 2 - A subgrid tilted by 30^O

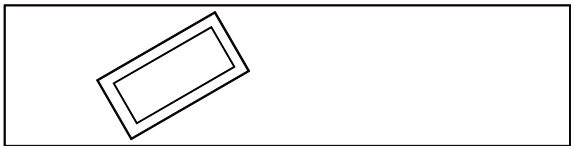

Figure 3 - Two Huygens surfaces surrounding the subgrid

III. PROPAGATION THROUGH A TILTED SUBGRID

As a first test, in order to gain confidence that the method is working correctly, a test structure consisting of a plane wave propagating through a subgrid region was used. If all is working perfectly then the existence of the subgrid would not affect the wave. For this test the size of the main grid is 3000mm x 750mm, the subgrid size is 600mm x 250mm and is centered at position 900mm x 375mm. The cell size in the main grid is 3mm and in the subgrid is 1mm. A plane wave was excited at the left hand end of the main grid with a single cycle sinusoid waveform having a width of 0.56ns corresponding to a center frequency of 1.8GHz. Figure 5 and Figure 6 show the wave before and after propagating through a subgrid tilted by 30^O. It can be seen that the pulse passes with very little distortion. In Figure 7 the pulse is shown as it passes through the subgrid. It can be seen that, as expected, the pulse is propagating at an angle of 30^O relative to the axes of the subgrid and is being correctly truncated at the top and bottom of the subgrid with just some very small spurious energy in the non-working regions outside.

The reflection from the subgrid was calculated by comparing the incident and reflected pulse at a probe point placed at a position of 300mm. The result is shown in Figure 8. It can be seen that the spurious reflection is less than -60dB and that it does not get worse when the grid is tilted.

IV. SCATTERING FROM A CYLINDER

As a second test, a cylinder was placed in the centre of the subgrid as shown in Figure 9. As before, a plane wave was launched from the left hand end of the box and the fields at the positions of the crosses were recorded. Because of symmetry, the angle at which the subgrid is tilted should not affect the result and any differences are due to approximation error in the subgrid interface. The reflected wave, as observed at the first probe point, is shown in Figure 10 for various angles of tilt and it can be seen that the agreement, although not perfect, is good. The transmitted wave, as observed at the second probe point, is

shown in Figure 11 and, again, the agreement is seen to be good.

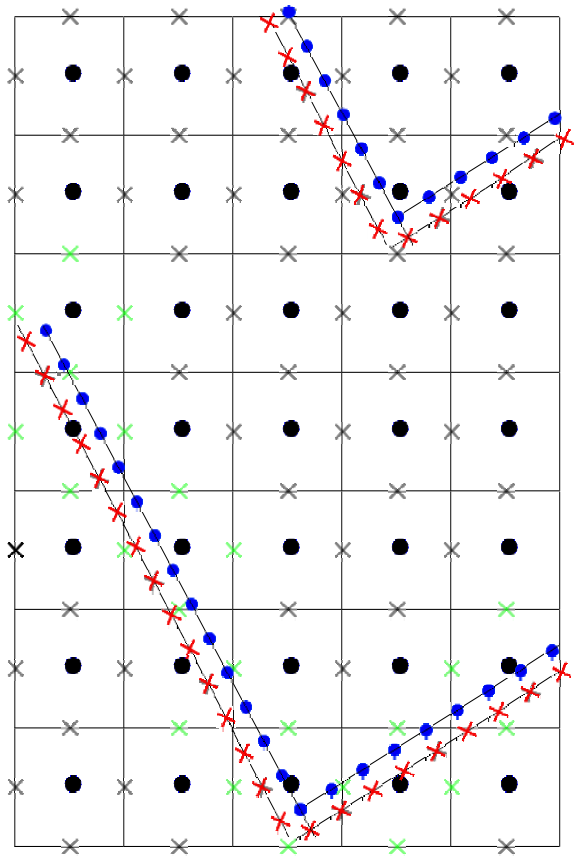

Figure 4 - Part of the boundary of the subgrid

Figure 5 - Pulse propagating before passing through the subgrid

Figure 6 - Pulse propagating after passing through a subgrid tilted by 30^{O}

Figure 7 - Pulse propagating in a subgrid tilted by 30^{O}

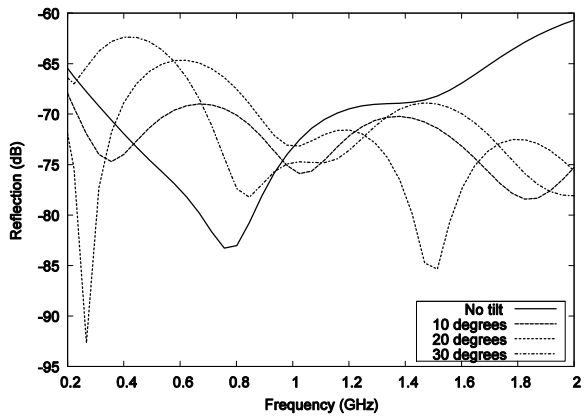

Figure 8 - Reflection from subgrids placed at various angles

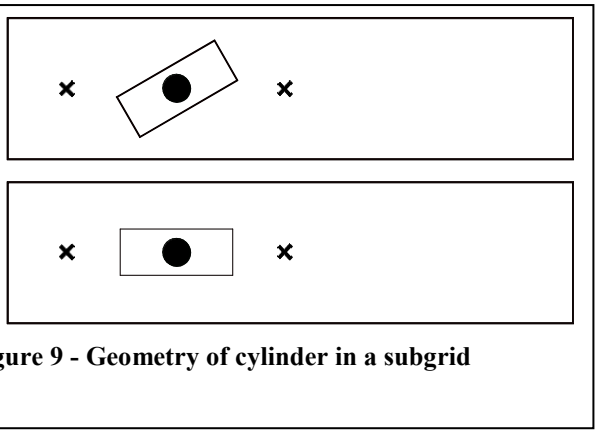

Figure 9 - Geometry of cylinder in a subgrid

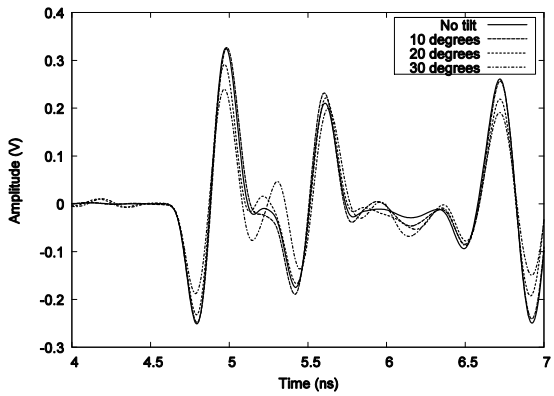

Figure 10 - E field amplitude at the first probe point

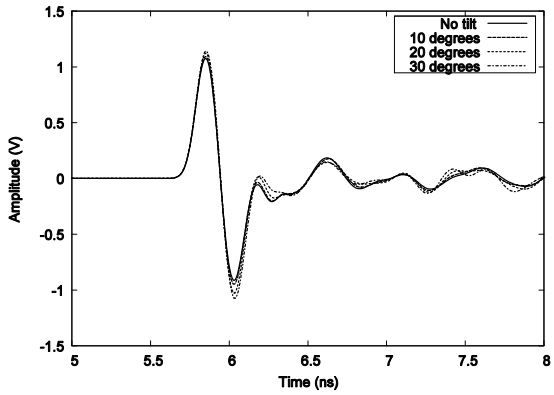

Figure 11 - E field amplitude at the second probe point

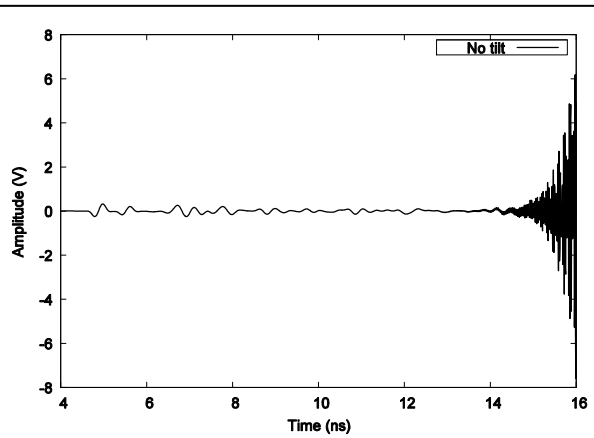

Figure 12 - Late time behavior of the E field amplitude at the first probe point. The gap is 3 and the subgrid is not tilted.

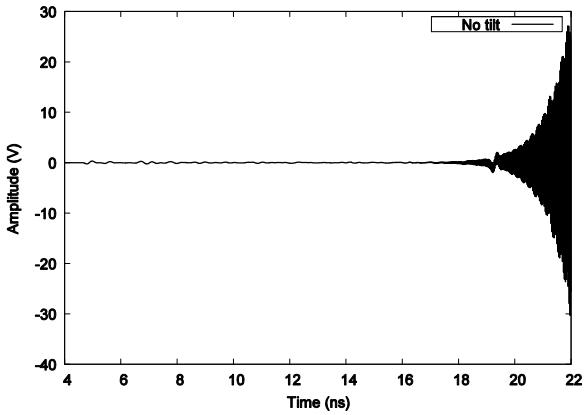

Figure 13 - Late time behavior of the E field amplitude at the first probe point. The gap is 5 and the subgrid is not tilted.

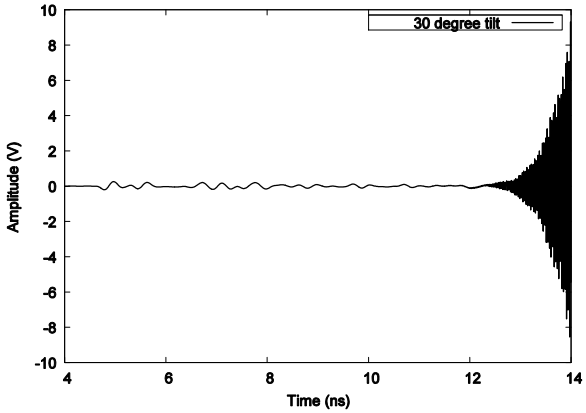

Figure 14 - Late time behavior of the E field amplitude at the first probe point. The gap is 3 and the subgrid is tilted by 30^{O}.

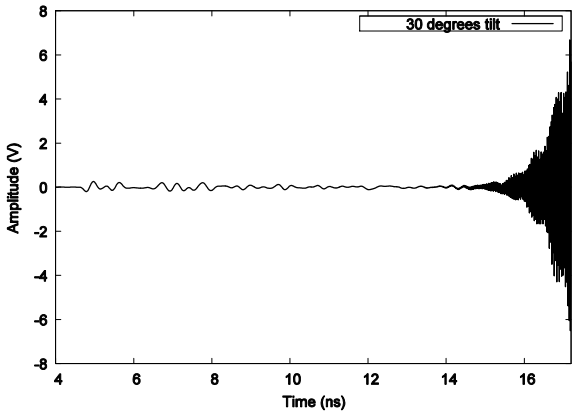

Figure 15 - Late time behavior of the E field amplitude at the first probe point. The gap is 5 and the subgrid is

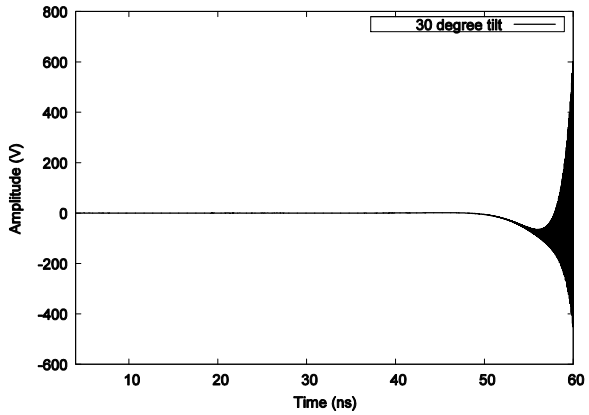

Figure 16 - Late time behavior of the E field amplitude at the first probe point. The gap is 3, the subgrid is tilted by 30^O and the time step is 70% of CFL for unmodified FDTD.

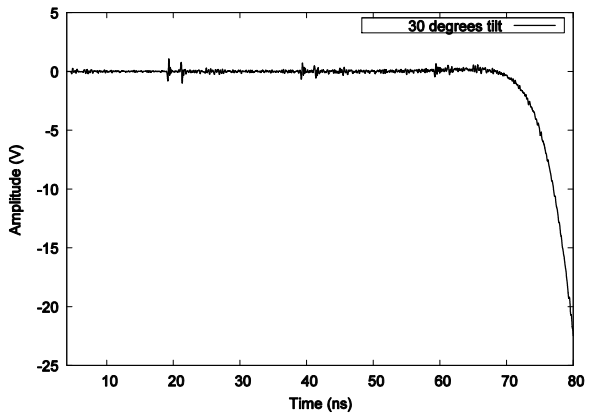

Figure 17 - Late time behavior of the E field amplitude at the first probe point. The gap is 5, the subgrid is tilted by 30^O and the time step is 70% of CFL for unmodified FDTD

V. STABILITY ISSUES

The method presented here unfortunately exhibits a similar problem of late time instability as the one reported in [4]. The reason for this is under investigation. Since one possible mechanism for instability is unwanted coupling between the inner and the outer surfaces, some experiments were done in order to ascertain the effect of the size of the gap between the inner and outer surfaces on the onset of instability.

It was found that by increasing the size of the gap from three main grid cell sizes to five, the onset of instability was delayed. This is demonstrated in Figure 12 and Figure 13 for the untilted case and Figure 14 and Figure 15 for the case where the grid is tilted by 30^O. It can be seen that in each case instability is significantly less severe with the wider gap.

Numerical experiments were also done to see the effect of reducing the time step. It was found that, although the instability was not removed, it could be substantially reduced by reducing the time step to 70% of the value required for stability in the unmodified FDTD algorithm. The results obtained are shown in Figure 16 and Figure 17 for a subgrid tilted by 30^O. It can be seen that the algorithm remains stable for a simulation time of about 4 times that which was observed with a time step close to the CFL limit. So far the results are empirical and it is not known whether there is a time step which will give complete stability. Such investigations will be part of future work.

It is expected that the use of spatial filters, such as described in [4], would be effective in mitigating instability and this will also be investigated as part of future work.

VI. CONCLUSIONS

In this contribution, a novel method for implementing tilted subgrids in the 2D FDTD method has been described and results presented which show that the method is effective. The method is readily extensible to 3D and that is the subject of ongoing research.

ACKNOWLEDGMENT

The author would like to thank his colleagues in the Centre for Communications Research for helpful discussions.

REFERENCES

[1] M. Klemm, J. Leendertz, D. Gibbins, I.J. Craddock, A. Preece, R. Benjamin, "Towards Contrast Enhanced Breast Imaging using Ultra-Wideband Microwave Radar System" , Radio and Wireless Symposium (RWS), 2010, pp. 516-519

[2] Sema Dumanli and Chris Railton, "Analysis of coupled tilted slot antennas in FDTD using a novel Time Domain Huygens method with application to Body Area Networks", IEEE Transactions on Antennas and Propagation, Vol. 60, No. 4, April 2012, pp 1987-1994.

[3] C Christodoulou, C. J. Railton, M. Klemm, D. Gibbins, I. J. Craddock, "Analysis of a UWB hemispherical antenna array in FDTD with a Time Domain Huygens method", IEEE Trans. On Antennas and Propagation, Vol. 60, No. 11, Nov. 2012, pp 5251-5258.

[4] Jean-Pierre Bérenger, "The Huygens subgridding for the numerical solution of the Maxwell equations", Journal of Computational Physics, 230 (2011) pp. 5635-5659.